Numerical study of discrete-velocity gases

Takaji Inamuro[a] and Bradford Sturtevant
Graduate Aeronautical Laboratories, California Institute of Technology, Pasadena, California 91125

(Received 15 March 1990; accepted 14 August 1990)

A finite-difference method for solving the discrete Boltzmann equations, which are the governing equations for a model gas in which molecules have many discrete velocities, is developed. The method is applied to three fundamental problems in rarefied gas flow to study the features of discrete-velocity gases: normal shock wave structure, heat transfer between two parallel plates, and two-dimensional vapor deposition. Two different discrete-velocity gas models are used.

I. INTRODUCTION

The discrete-velocity gas, in which the velocities of molecules are restricted to a finite set of vectors, has been used to solve the Boltzmann equation by several authors.[1-7] The discrete-velocity gas is useful because for binary collisions the difficult integral collision term in the Boltzmann equation reduces to a series of quadratic terms. The Boltzmann equation is thus reduced to a system of simultaneous nonlinear first-order differential equations called the discrete Boltzmann equations. The discrete Boltzmann equations can be solved analytically for gases with few velocities. However, numerical computation is required in cases when there are many discrete velocities.

Broadwell[1,2] used two simple models in which the velocities had only a single speed. He applied the models to the study of shock wave structure, Couette flow, and Rayleigh flow. Gatignol[3] used six coplanar velocities to study shock wave structure. She also studied Couette flow with four coplanar velocities.[4,5] Cabannes[6] used a multispeed model that had 14 velocities to study Couette flow. Nadiga *et al.*[8] proposed a multispeed cellular automaton and studied heat conduction and shock wave behavior. Despite the fact that these models use only a few velocities, they give a simple physical interpretation of the phenomena. However, a large number of velocities are required to obtain accurate results. So far there has been no attempt to solve the discrete Boltzmann equations using more velocities.

Goldstein *et al.*[9] used a large number of discrete velocities in the direct simulation Monte Carlo method (DSMC) and obtained accurate results for shock wave structure. They showed that fewer than ten values of each component of molecular velocity were required to obtain accurate results. Thus it is of interest to solve the discrete Boltzmann equations numerically using a large number of molecular velocities. In fact, with present-day supercomputers, it is possible to use thousands of velocities in solving the discrete Boltzmann equations. In the present paper, a numerical method for solving the discrete Boltzmann equations is proposed, and the features of discrete-velocity gases are studied in calculations of fundamental problems of rarefied gas flow. Three problems are calculated: normal shock wave structure, heat transfer between two parallel plates, and two-dimensional vapor deposition. Two different discrete-velocity gas models are used.

[a] Permanent address: Advanced Technology Research Center, Mitsubishi Heavy Industries, Ltd., Yokohama 236, Japan.

II. FORMULATION

A. Basic equation

A gas composed of identical hard sphere molecules whose velocities are restricted to a finite set of p vectors: ξ_1, $\xi_2,\ldots,\xi_p$ is considered. The behavior of the gas is described by the discrete Boltzmann equations,[7]

$$\frac{\partial N_i}{\partial t} + \xi_i \cdot \nabla N_i = \sum_{j=1}^{p} \sum_{(k,l)} A_{ij}^{kl}(N_k N_l - N_i N_j), \quad i = 1,2,\ldots,p, \tag{1}$$

where $N_i(\mathbf{x},t)$ is the number density of the molecules with velocity ξ_i at the point $\mathbf{x}$ and at time t. The transition probability A_{ij}^{kl} is given by

$$A_{ij}^{kl} = \pi d^2 |\xi_i - \xi_j| a_{ij}^{kl}, \tag{2a}$$

$$\sum_{(k,l)} a_{ij}^{kl} = 1, \tag{2b}$$

where d is the diameter of the molecule and a_{ij}^{kl} is the probability with which the pair of molecules with velocities ξ_i, ξ_j before collision results in the pair of molecules with velocities ξ_k, ξ_l after collision. For hard sphere molecules, all possible pairs after collision are obtained with the same probability. Therefore the coefficient a_{ij}^{kl} is determined by computing the number of pairs that can be obtained after collision.

The macroscopic variables, number density n, gas velocity $\mathbf{u}$, temperature T, and heat flux vector $\mathbf{q}$ are given by

$$n = \sum_{i=1}^{p} N_i, \tag{3a}$$

$$\mathbf{u} = \frac{1}{n} \sum_{i=1}^{p} N_i \xi_i, \tag{3b}$$

$$T = \frac{1}{3R}\left[\frac{1}{n}\left(\sum_{i=1}^{p} N_i \xi_i^2\right) - \mathbf{u}^2\right], \tag{3c}$$

$$\mathbf{q} = \frac{m}{2} \sum_{i=1}^{p} N_i (\xi_i - \mathbf{u})^2 (\xi_i - \mathbf{u}), \tag{3d}$$

 0899-8213/90/122196-08$02.00

where R is the specific gas constant and m is the particle mass.

B. Equilibrium state

It is often necessary to specify conditions at equilibrium, for example, to apply boundary conditions. Here we use approximations to the equilibrium state. It is shown by Gatignol[3] that in the equilibrium state the number densities N_i depend only on the macroscopic variables. Nadiga *et al.*[8] derive the equilibrium state for a two-dimensional gas with nine velocities. It is, however, difficult to obtain analytically the relations between N_i and the macroscopic variables for discrete-velocity gases with more velocities. Goldstein *et al.*[9] show by Monte Carlo simulation that the equilibrium distribution of number densities for the discrete-velocity gas with a moderate number of velocities agrees extremely well with the Maxwellian distribution for the continuous velocity gas. Therefore, for the purposes of this paper, we use the Maxwellian distribution for the equilibrium state of the discrete-velocity gas. Assuming that the discrete velocities are equally distributed in velocity space, the number densities for an equilibrium state with temperature T_0, number density n_0, and velocity $\mathbf{u}_0$ are given by

$$N_{ei} = \frac{n_0}{\sum_{j=1}^{p} \exp[-(\xi_j - \mathbf{u}_0)^2/2RT_0]} \times \exp\left(-\frac{(\xi_i - \mathbf{u}_0)^2}{2RT_0}\right). \tag{4}$$

We note that the number densities N_{ei} given by Eq. (4) have the following relations:

$$\sum_{i=1}^{p} N_{ei} = n_0, \tag{5a}$$

$$\frac{1}{n_0}\sum_{i=1}^{p} N_{ei}\xi_i \approx \mathbf{u}_0, \tag{5b}$$

$$\frac{1}{3R}\left[\frac{1}{n_0}\left(\sum_{i=1}^{p} N_{ei}\xi_i^2\right) - \mathbf{u}_0^2\right] \approx T_0. \tag{5c}$$

The approximations in Eqs. (5b) and (5c) become exact as the number of velocities approaches infinity.

A method for obtaining more accurate equilibrium state of discrete-velocity gases and calculated results will be reported in the future.

C. Collision relation

The collision relations of the discrete-velocity gas are calculated in the following way. For simplicity we use the example of a two-dimensional gas. The generalization to a three-dimensional gas is straightforward. Figure 1 shows an example of a collision in which a pair of molecules with velocities ξ_i, ξ_j before collision are replaced by one of several possible pairs after collision. The conservation of momentum and energy requires that the magnitude of the precollision relative velocity is the same as that of the post-collision velocity and that the centers of the two relative velocities coincide. All possible pairs after collision are shown in Fig. 1 by open circles connected by dashed lines. As mentioned before, for the hard sphere molecules all possible pairs after collision are obtained with the same probability. Thus the coefficients a_{ij}^{kl} are calculated by

$$a_{ij}^{kl} = 1/M_{ij}, \tag{6}$$

where M_{ij} is the number of all possible pairs after collision, corresponding to the precollision velocities ξ_i, ξ_j, including a trivial collision in which the post-collision velocities are the same as the precollision velocities.

III. METHOD OF COMPUTATION

A. Finite-difference method

The discrete Boltzmann equations (1) are solved numerically by using a finite-difference method. We use an implicit method, except that the collision terms are evaluated explicitly. For simplicity we present only a one-dimensional spatial case (x: the spatial coordinate) in the following. The finite-difference scheme for Eqs. (1) is as follows:

$$\frac{N_i^{r+1} - N_i^r}{\Delta t} + \xi_{ix} D_x N_i^{r+1} = \sum_{j=1}^{p} \sum_{(k,l)} A_{ij}^{kl}(N_k^r N_l^r - N_i^{r+1} N_j^r), \quad i = 1,2,\ldots,p, \tag{7}$$

where Δt is the increment of time t; N_i^r, N_i^{r+1} are approximations to $N_i(x, r\,\Delta t)$, $N_i[x,(r+1)\Delta t]$; ξ_{ix} is the x component of ξ_i, and D_x is the spatial differencing operator. The spatial differencing operator D_x is approximated by the following upwind schemes in order to ensure numerical stability. The first-order upwind scheme for D_x:

$$D_x N_i^{r+1} = \begin{cases} (N_{is}^{r+1} - N_{is-1}^{r+1})/\Delta x, & \text{for } \xi_{ix} > 0, \\ (N_{is+1}^{r+1} - N_{is}^{r+1})/\Delta x, & \text{for } \xi_{ix} < 0; \end{cases} \tag{8}$$

the second-order upwind scheme for D_x:

$$D_x N_i^{r+1} = \begin{cases} (3N_{is}^{r+1} - 4N_{is-1}^{r+1} + N_{is-2}^{r+1})/2\,\Delta x, & \text{for } \xi_{ix} > 0, \\ (-3N_{is}^{r+1} + 4N_{is+1}^{r+1} - N_{is+2}^{r+1})/2\,\Delta x, & \text{for } \xi_{ix} < 0; \end{cases} \tag{9}$$

and the third-order upwind scheme for D_x:

$$D_x N_i^{r+1} = \begin{cases} \dfrac{11N_{is}^{r+1} - 18N_{is-1}^{r+1} + 9N_{is-2}^{r+1} - 2N_{is-3}^{r+1}}{6\,\Delta x}, & \text{for } \xi_{ix} > 0, \\ \dfrac{-11N_{is}^{r+1} + 18N_{is+1}^{r+1} - 9N_{is+2}^{r+1} + 2N_{is+3}^{r+1}}{6\,\Delta x}, & \text{for } \xi_{ix} < 0. \end{cases} \tag{10}$$

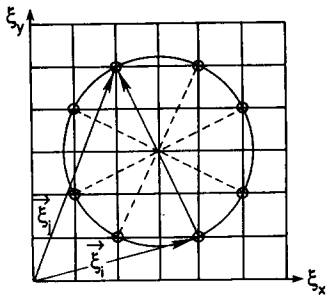

FIG. 1. Collision relations of the discrete-velocity gas.

In Eqs. (8)–(10), Δx is the increment of the variable x and N_{is}^{r+1}, N_{is-1}^{r+1},..., are approximations to $N_i[s\,\Delta x,(r+1)\Delta t\,]$, $N_i[(s-1)\Delta x,(r+1)\Delta t\,]$,... .

B. Discrete-velocity gas model

We can choose any set of vectors for the discrete velocities. In the following calculations we use two models. One model illustrated by a two-dimensional gas is shown in Fig. 2(a). In this model the velocities are set up equally in velocity space, including points along each velocity axis. This model is used frequently for discrete-velocity gases. However, as pointed out in Ref. 6, if the molecules reflect diffusely at the wall (e.g., the wall along the ξ_y axis), the molecules with velocities along the ξ_y axis are isolated from the boundary condition because they never collide with the wall. Thus these molecules cause error at the wall. To avoid this defect we use the other model shown in Fig. 2(b). In this model the velocities occur at half-integer locations. We hereafter refer to the former model as the odd model (O) and to the latter model as the even model (E). Comparison of the results by both models is shown in Sec. IV.

C. Storing of collision relation

The collision relations of Eq. (7) are precalculated and are stored in a lookup table. The table contains the post-collision pairs (k,l) corresponding to a given precollision pair (i_0,j), where i_0 is a representative point in the velocity space (e.g., $\xi_{i_0}=\mathbf{0}$). The possible outcomes of an (i',j') collision are then found from the points in the lookup table corresponding to the point (i_0,j), which has the same relative velocity as (i',j') (i.e., $\xi_j-\xi_{i_0}=\xi_{j'}-\xi_{i'}$). Finally, the values (k',l') are found by translating the collision sphere back by adding the velocity $(\xi_{i'}-\xi_{i_0})$ to ξ_k and ξ_l.

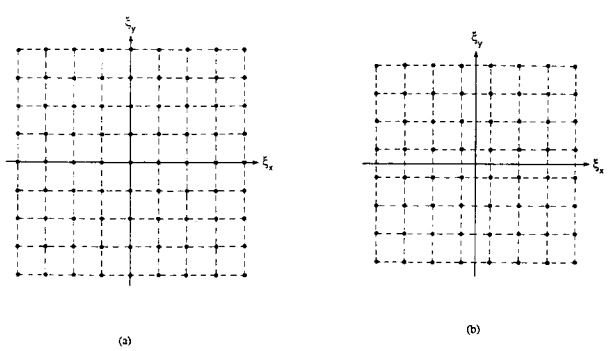

FIG. 2. Discrete-velocity gas model: (a) odd model; (b) even model.

D. Symmetry of number densities

We can save computation time for a one- or two-dimensional problem by using the symmetry relation of the number densities of molecules: For one dimension

$$N_k(\mathbf{x},t)=N_l(\mathbf{x},t), \tag{11}$$

with

$$\xi_{kx}=\xi_{lx},\quad (\xi_{ky}^2+\xi_{kz}^2)^{1/2}=(\xi_{ly}^2+\xi_{lz}^2)^{1/2}, \tag{12}$$

where k and l are two different i's in $i=1,2,...,p$. For two dimensions Eq. (11) is satisfied with

$$\xi_{kx}=\xi_{lx},\quad \xi_{ky}=\xi_{ly}\quad |\xi_{kz}|=|\xi_{lz}|. \tag{13}$$

These relations are used in the following calculations.

IV. RESULTS AND DISCUSSION

In order to examine the features of the discrete-velocity gas three problems are studied.

A. Shock wave structure

We first calculate the structure of a normal shock wave. Consider two different equilibrium states, which are distance L apart and are separated by the normal shock wave. The equilibrium states are composed of number density n_1, temperature T_1, and mean velocity u_1 for the upstream side $(x=L)$ and of n_2, T_2, and u_2 for the downstream side $(x=0)$. In the following calculation we choose $L/\lambda_1=15$ (λ_1 is the mean-free path of the upstream state), $n_2/n_1=u_1/u_2=2.7027$, and $T_2/T_1=2.7981$, corresponding to upstream Mach number $M_1=2.5$ for gas of specific heat ratio $\gamma=\frac{5}{3}$. In order to obtain a reliable solution we need several cells in a mean-free path. So, we divide the distance L into 60 equal cells ($x=s\,\Delta x, s=0,1,...,60$). We use the discrete-velocity gas models shown in Table I. The initial conditions are as follows: the number densities are equal to those of the downstream equilibrium state for $x\leqslant 26\,\Delta x$ and to those of the upstream equilibrium state for $x\geqslant 27\,\Delta x$.

We first show in Fig. 3 comparisons of results obtained using the different spatial difference schemes [Eqs. (8)–(10)]. The results from the second- and the third-order schemes coincide extremely well, while the results from the first-order scheme deviate from those results because of numerical dissipation resulting from truncation errors. From these results we can see that the second-order scheme is sufficient to obtain accurate results for the present problem. Thus we use the second-order scheme in the following calculations.

Figure 4 shows the calculated results from the various discrete-velocity gas models. The result from model O7 is much different from those of other models. In particular, the macroscopic values of model O7 in the upstream and downstream state deviate from those of the other models. This is probably because the number densities of molecules for the equilibrium state of model O7 are different from the Maxwellian distribution for continuous-velocity gases. Further-

TABLE I. Discrete-velocity gas models for the shock wave problem.

Model	Number of velocities	$\Delta\xi/\sqrt{2RT_1}$	ξ_x	ξ_y and ξ_z
O7	$7\times7\times7$	1.2857	$j\Delta\xi$, $-2\leqslant j\leqslant4$	$j\Delta\xi$, $-3\leqslant j\leqslant3$
O9	$9\times9\times9$	1.0	$j\Delta\xi$, $-3\leqslant j\leqslant5$	$j\Delta\xi$, $-4\leqslant j\leqslant4$
O11	$11\times11\times11$	0.818 18	$j\Delta\xi$, $-4\leqslant j\leqslant6$	$j\Delta\xi$, $-5\leqslant j\leqslant5$
O13	$13\times13\times13$	0.692 31	$j\Delta\xi$, $-5\leqslant j\leqslant7$	$j\Delta\xi$, $-6\leqslant j\leqslant6$
E10	$10\times10\times10$	0.9	$(j+\frac{1}{2})\Delta\xi$, $-4\leqslant j\leqslant5$	$(j+\frac{1}{2})\Delta\xi$, $-5\leqslant j\leqslant4$

more, it can be seen that the shock wave becomes thicker as the number of velocities is fewer. As pointed out in Ref. 9, with few velocities the excess of the trivial collision (the collision in which the post-collision velocities are the same as the precollision velocities) has the effect of artificially increasing the diffusivity of the gas, and this effect causes an increase of the shock wave thickness. From Fig. 4 we can see that the results are almost converged in the 11-velocity calculation (model O11 yields 1% accuracy compared with model O13). Of course, more velocities are needed for higher Mach numbers. It is confirmed from additional calculations that more than 13 velocities in each component are necessary for $M_1 = 5.0$. Comparison of the results from the odd and the even models is shown in Fig. 5. Both results agree very well (within 0.5%), so there is no distinction between the models in this problem. Finally, the present results are compared with those of the DSMC by Goldstein[10] in Fig. 6. They are in good agreement.

The above calculations were carried out on a Cray Y-MP/832, and, for 60 time steps, required 182 sec for model O9, 686 sec for model O11, and 2098 sec for model O13. The variations of macroscopic variables at all cells were less than 2.2×10^{-4} at the last time step. In model O9, there are a total of 615 773 quadratic terms on the right-hand side (rhs) of the 135 discrete Boltzmann equation (1), i.e., an average of 4561 collision terms in each equation. On the other hand, in model O13 there are 7 479 917 terms on the rhs of 364 equations, averaging 20 549 per equation. It is clear that great savings in computation time could be realized if a scheme were used in which only those terms representing collisions that occur with finite probability are actually computed.

B. Heat transfer between two parallel plates

Consider a gas between two parallel infinite plates that are distance of L apart and have different uniform temperature T_1 (at $x = 0$) and T_2 (at $x = L$). Molecules reflect diffusely from the plates. We present results of calculations of fluid properties and heat flux for temperature ratio $T_2/T_1 = 2.0$ and Knudsen number $\mathrm{Kn} = \lambda_0/L = 0.1$, where λ_0 is defined by the reference number density n_0. In the following calculations, the distance L is divided into 60 equal cells and the discrete-velocity gas models shown in Table II are used. Also, we assume that initially the gas between the plates has the temperature $(T_1 + T_2)/2$ and the number density is n_0.

Figure 7 shows a comparison of the temperature distributions obtained using the various discrete-velocity gas models. The difference between the result from model E6 and those of other models is large at the low-temperature

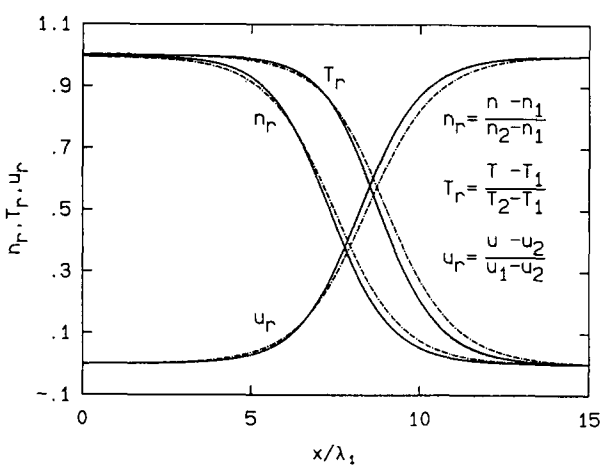

FIG. 3. Comparison of results of $M_1 = 2.5$ obtained by using the different spatial differences schemes: —, third-order scheme; ---, second-order scheme; —·—, first-order scheme. The model O9 for the discrete-velocity gas is used.

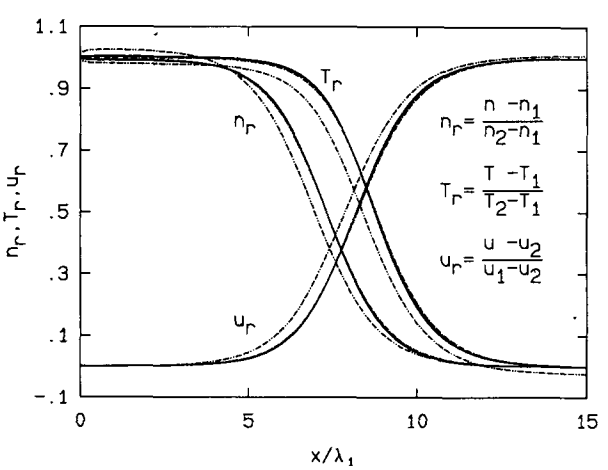

FIG. 4. Shock wave structure of $M_1 = 2.5$: —, model O13; ---, model O11; —·—, model O9; ——, model O7.

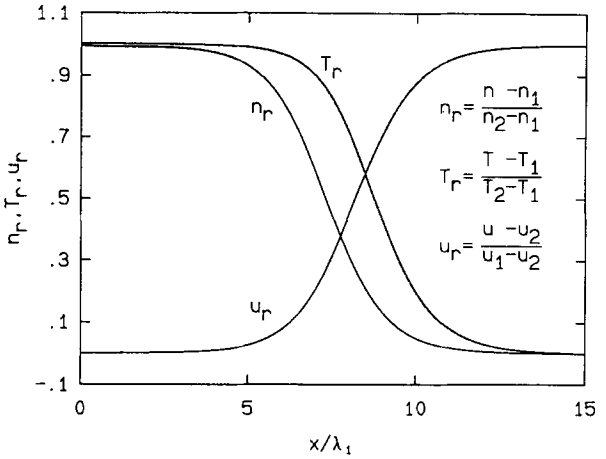

FIG. 5. Comparison of results of $M_1 = 2.5$ from the odd model and the even model: —, model O11; ---, model E10.

wall. Again, this difference comes mainly from errors in the assumed equilibrium expressions [Eq. (4)]. This difference is larger at the low-temperature wall than at the high-temperature wall because the effective velocities are fewer at the low-temperature wall. It is seen that the results converge when more than ten velocities in each component are used. Model E10 yields results within 0.3% of those of model E12. In other calculations it was found that more than 12 velocities in each component are necessary for the case of $T_2/T_1 = 4.0$. Figure 8 shows a comparison of the results from the odd and even models. In this problem, these models differ at both walls. The temperature jump at the wall is larger for the odd model than for the even model. As explained before, in the odd model the molecules with the velocities along the wall are independent of the boundary condition at the wall. Those molecules cannot transfer the wall temperature to the molecules in the inner region. Thus the temperature jump becomes large in the odd model. The heat flux for each model is shown in Table III. The heat fluxes of

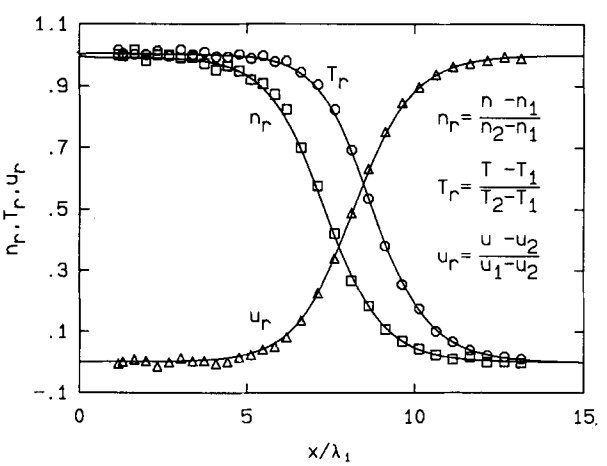

FIG. 6. Comparison of the present results of $M_1 = 2.5$ with those by DSMC (Ref. 10): —, model O13; ○, □, △, DSMC.

TABLE II. Discrete-velocity gas models for the heat transfer problem.

Model	Number of velocities	$\Delta\xi/\sqrt{2RT_1}$	ξ_x, ξ_y, and ξ_z
E6	$6\times6\times6$	1.3333	$(j+\frac{1}{2})\Delta\xi$, $-3\leqslant j\leqslant 2$
E8	$8\times8\times8$	1.0	$(j+\frac{1}{2})\Delta\xi$, $-4\leqslant j\leqslant 3$
E10	$10\times10\times10$	0.8	$(j+\frac{1}{2})\Delta\xi$, $-5\leqslant j\leqslant 4$
E12	$12\times12\times12$	0.666 67	$(j+\frac{1}{2})\Delta\xi$, $-6\leqslant j\leqslant 5$
O11	$11\times11\times11$	0.727 27	$j\Delta\xi$, $-5\leqslant j\leqslant 5$

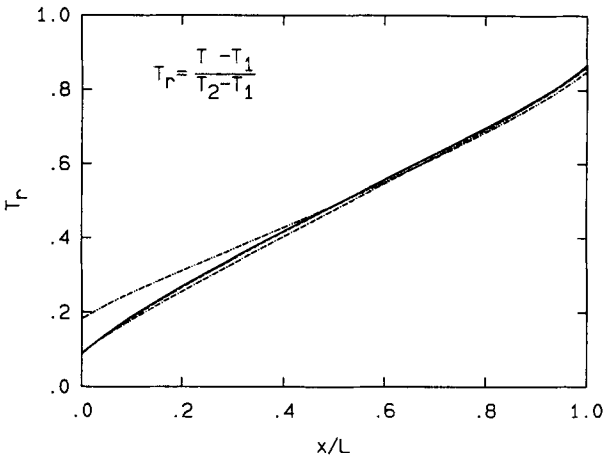

FIG. 7. Temperature distribution of $T_2/T_1 = 2.0$: —, model E12; ---, model E10; ——, model E8; ——, model E6.

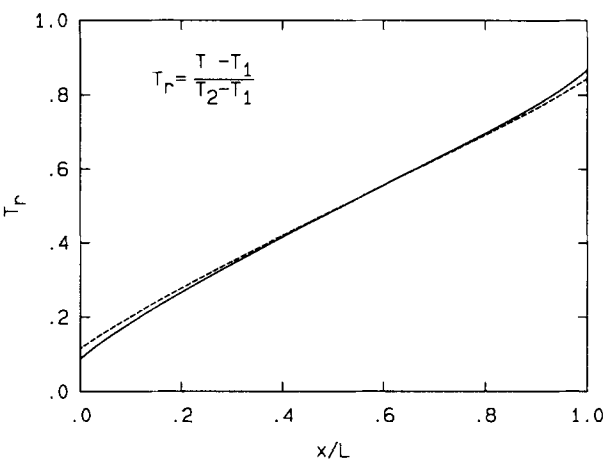

FIG. 8. Comparison of results of $T_2/T_1 = 2.0$ from the odd model and the even model: —, model E10; ---, model O11.

TABLE III. Heat flux q_x.

Model	$q_x/[(\sqrt{2}mn_0(RT_1)^{3/2}]$
E6	0.227
E8	0.193
E10	0.189
E12	0.187
O11	0.188

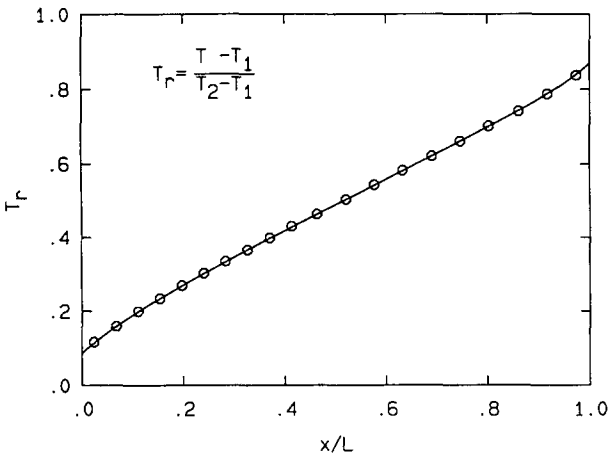

FIG. 9. Comparison of the present result of $T_2/T_1 = 2.0$ with that by DSMC (Ref. 11): —, model E12; O, DSMC.

models E10 and O11 agree, despite the difference in the temperature distributions (Fig. 8), since the molecules that have the velocities along the wall and cause error in the calculations of temperature do not contribute to heat flux. Finally, we show in Fig. 9 a comparison between a temperature distribution from the present results and one calculated by the DSMC.[11] The results are in fairly good agreement.

The computation time for 100 time steps was 112 sec for model E8, 506 sec for model E10, and 1756 sec for model E12 on a Cray Y-MP/832. The variations of macroscopic variables at all cells were less than 1.8×10^{-4} at the last time step.

C. Two-dimensional vapor deposition

Consider a two-dimensional chamber shown in Fig. 10. This is a model of a vacuum vapor deposition apparatus.[12] Here $\overline{AB}$ is the evaporation surface; molecules reflected from this surface are assumed to posses a stationary Maxwellian distribution corresponding to a saturated gas of number density n_0 at the surface temperature T_0. Also, $\overline{DE}$ is the deposition surface, on which all incident molecules are deposited; $\overline{EA}$ is a surface of symmetry, from which molecules reflect specularly. The remaining walls are diffuse reflection surfaces at temperature T_0. The dimensions of the chamber are $H/L = 1.0$ and $b/L = 0.5$. The Knudsen number is $\mathrm{Kn} = \lambda_0/L = 0.1$, where λ_0 is the mean-free path of the molecules at the stationary equilibrium state with the temperature T_0 and the number density n_0. The square region is divided equally into 10×10 cells and the discrete-velocity gas models shown in Table IV are used.

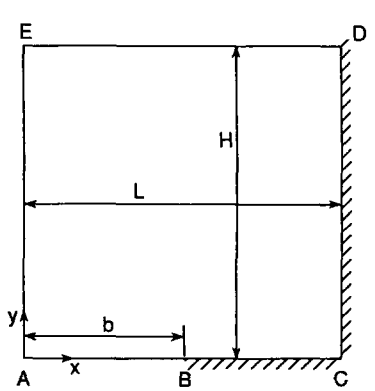

FIG. 10. Model chamber of vacuum vapor deposition.

The calculated results are shown in Fig. 11. It is seen that the velocity vectors are similar in the three cases, while the density contours are different. In the results of models E10 and E20, the contours far from the evaporation surface are distorted and the density gradients along the symmetry surface are steep. The reason for these distinctions is probably that models E10 and E20 have too few discrete directions of velocities, particularly few directions toward the deposition surface, to yield the correct structure of the flow field. The distortion becomes smaller and the gradient becomes gentler in the results of model E40 than those of other models. Figure 12 shows the mass flux distribution on the deposition surface. As the number of velocities decreases the distribution becomes more nonuniform, consistent with the coarser resolution of direction with fewer velocities. Evidently, the homogenizing effect of collisions is not sufficient to smooth out the mass flux distributions when there are few velocities.

The computation time for 60 time steps required 1734 sec for model E10, 3124 sec for model E20, and 6057 sec for model E40 on a Cray Y-MP/832. The variations of macroscopic variables at all cells were less than 6.9×10^{-4} at the last time step.

V. CONCLUDING REMARKS

Calculations of the flow of rarefield discrete-velocity gases show that (i) for typical one-dimensional problems, about ten values of each component of molecular velocity are necessary to obtain accurate results, (ii) the even model of discrete-velocity gases is useful for problems with diffusely reflecting walls, and (iii) the fact that direction as well as magnitude in velocity space is discretized can affect results in two- or three-dimensional problems.

Similar results are obtained in Refs. 8, 9, and 11 in which motions of discrete-velocity gases are directly simulated using a multicomputer. As already stated, the present results for heat transfer between two parallel plates are in good agreement with those of Ref. 11. Although the computers used were different (Cray Y-MP/832 versus 128 processor Symult 2010), both implementations yield similar performance; around 750 million quadratic terms per hour are evaluated in the present method while 220 million collisions per hour are performed in the multicomputer simulations. Extensions of the work carried out in the authors' laboratory reported in Ref. 8 have not progressed sufficiently to permit quantitative comparison of results. The advantage of the present approach over Monte Carlo direct simulation is that the results are noise free and there are no sampling errors. In general, however, the present method requires more computation time than the other methods if more velocities are used, since the computation time of the present method is in

TABLE IV. Discrete-velocity gas models for the two-dimensional vapor deposition problem.

Model	Number of velocities	$\Delta\xi/\sqrt{2RT_0}$	ξ_x	ξ_y	ξ_z
E10	$10\times10\times10$	0.667	$(j+\frac{1}{2})\Delta\xi$, $-5\leqslant j\leqslant 4$	$(j+\frac{1}{2})\Delta\xi$, $-5\leqslant j\leqslant 4$	$(j+\frac{1}{2})\Delta\xi$, $-5\leqslant j\leqslant 4$
E20	$20\times10\times10$	0.667	$\frac{1}{2}(j+\frac{1}{2})\Delta\xi$, $-10\leqslant j\leqslant 9$	$(j+\frac{1}{2})\Delta\xi$, $-5\leqslant j\leqslant 4$	$(j+\frac{1}{2})\Delta\xi$, $-5\leqslant j\leqslant 4$
E40	$40\times10\times6$	0.667	$\frac{1}{4}(j+\frac{1}{2})\Delta\xi$, $-20\leqslant j\leqslant 19$	$(j+\frac{1}{2})\Delta\xi$, $-5\leqslant j\leqslant 4$	$(2j+1)\Delta\xi$, $-3\leqslant j\leqslant 2$

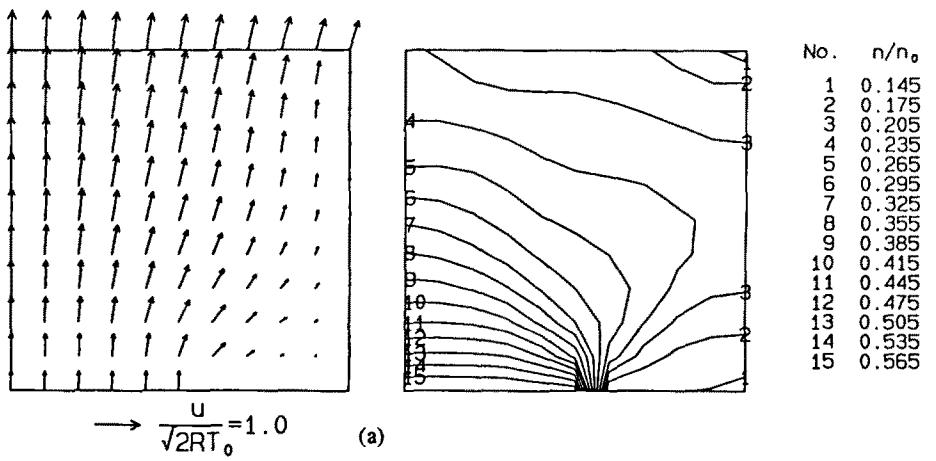

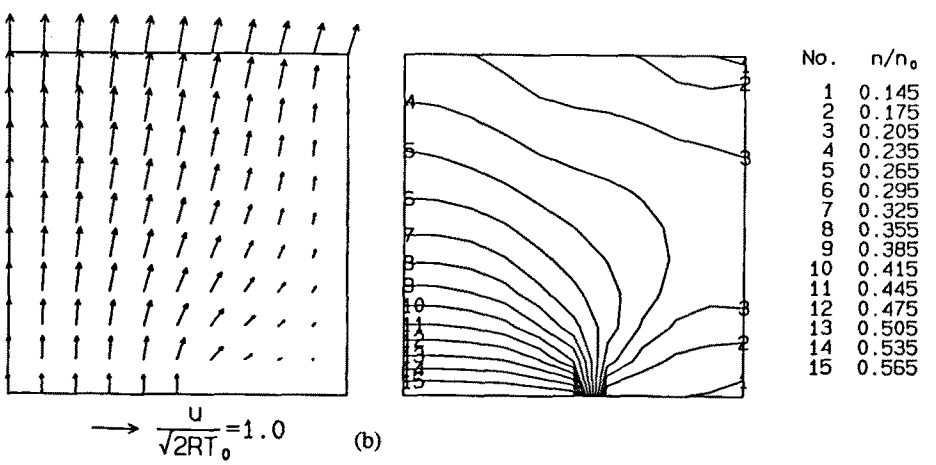

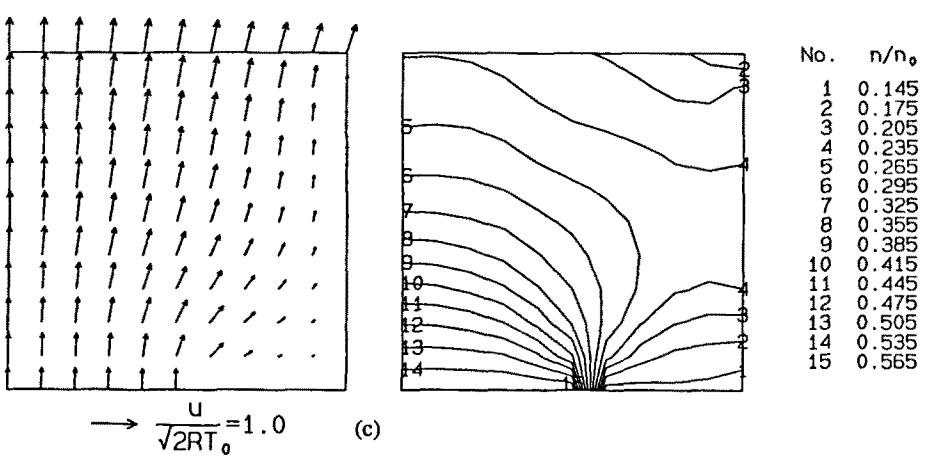

FIG. 11. Velocity vectors and density contours: (a) model E10; (b) model E20; and (c) model E40.

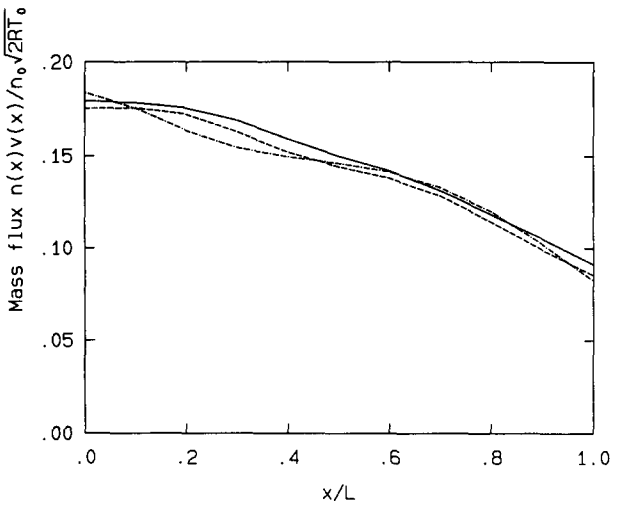

FIG. 12. Mass flux distribution on deposition surface: —, model E40; ---, model E20; —·—, model E10.

proportion to p^2, while those of the other methods are in proportion to the number of simulation particles. Further work remains in order to reduce computation time.

ACKNOWLEDGMENTS

The computations reported here were performed on the Cray Y-MP/832 of NAS System at NASA Ames Research Center through support of the NASA Langley Research Center.

This work was supported by Mitsubishi Heavy Industries, Ltd. and Office of Scientific Research, United States Air Force through Contract No. AFOSR-87-0155.

[1] J. E. Broadwell, J. Fluid Mech. **19**, 401 (1964).
[2] J. E. Broadwell, Phys. Fluids **7**, 1243 (1964).
[3] R. Gatignol, Phys. Fluids **18**, 153 (1975).
[4] R. Gatignol, Phys. Fluids **20**, 2022 (1977).
[5] R. Gatignol, in *Rarefied Gas Dynamics*, edited by R. Campargue (Commissariat a l'Energie Atomique, Paris, 1977), Vol. I, p. 195.
[6] H. Cabannes, J. Fluid Mech. **76**, 273 (1976).
[7] H. Cabannes, *The Discrete Boltzmann Equation, Theory and Applications*, Lecture Notes (Univ. of California Press, Berkeley, CA, 1980).
[8] B. T. Nadiga, J. E. Broadwell, and B. Sturtevant, in *Rarefied Gas Dynamics: Theoretical and Computational Techniques*, edited by E. P. Muntz, D. P. Weaver, and D. H. Campbell (AIAA, Washington, DC, 1989), p. 155.
[9] D. B. Goldstein, B. Sturtevant, and J. E. Broadwell, in *Rarefied Gas Dynamics: Theoretical and Computational Techniques*, edited by E. P. Muntz, D. P. Weaver, and D. H. Campbell (AIAA, Washington, DC, 1989), p. 100.
[10] D. B. Goldstein (private communication).
[11] D. B. Goldstein and B. Sturtevant, AIAA Paper No. 89-1668, 1989.
[12] T. Inamuro, in *Rarefied Gas Dynamics: Physical Phenomena*, edited by E. P. Muntz, D. P. Weaver, and D. H. Campbell (AIAA, Washington, DC, 1989), p. 418.